Supplemental material

Michels et al., https://doi.org/10.1084/jem.20180823

A

donor	gender	age	location	source
#1	male	73	ascending colon	resection, tumor-adjacent mucosa
#2	male	49	descending colon	biopsy, preemptive colonoscopy
#3	female	60	sigmoid colon	resection, tumor-adjacent mucosa

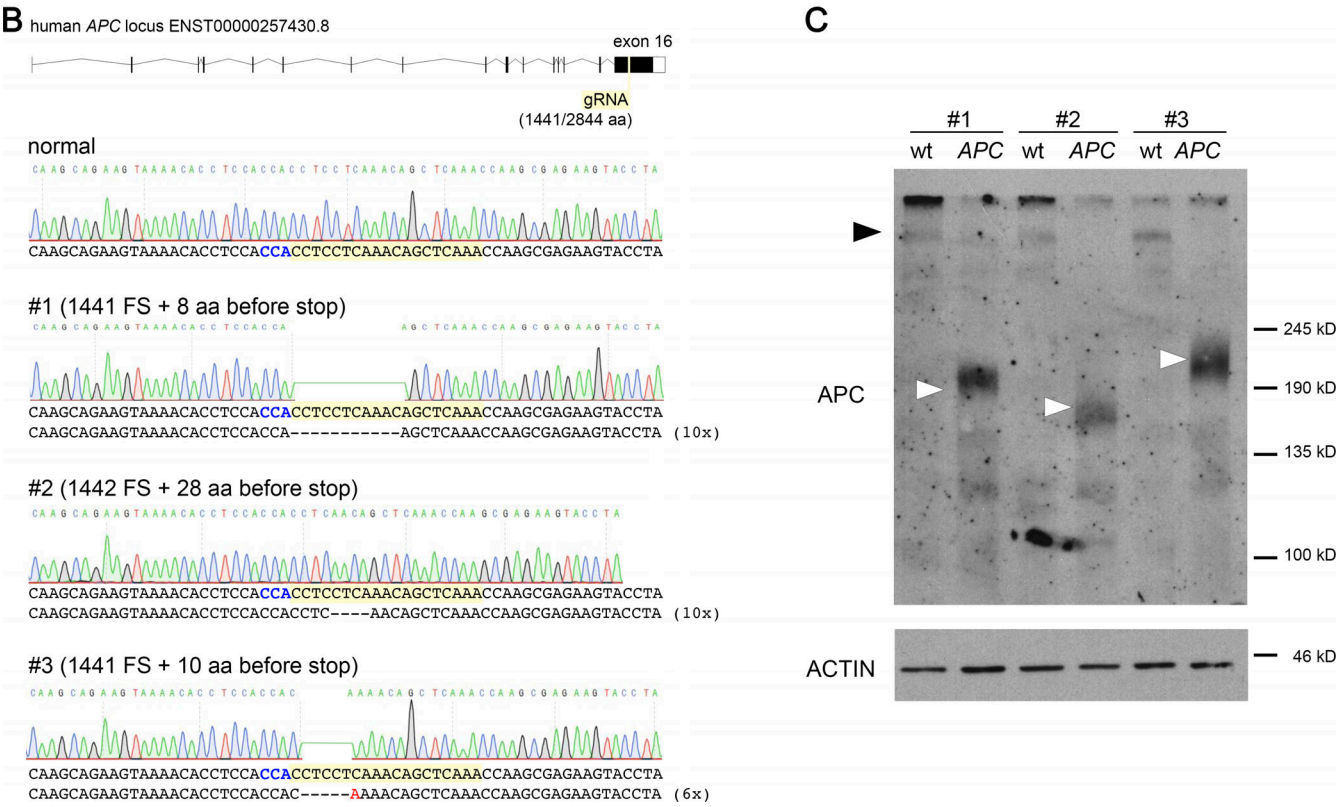

Figure S1. **Molecular characterization of CRISPR/Cas9 engineered organoids. (A)** Characteristics of the organoid lines used in this study. **(B)** Sanger sequencing for validation of CRISPR/Cas9-induced *APC*-KO mutations. Top scheme indicates the gRNA binding site in exon 16 of the human *APC* gene. The position corresponds to the codon for aa 1,441 of the APC protein (2,844 aa in total). Below, the sequencing spectrograms are shown in WT cells and all three lines. The PAM and gRNA target sequences are indicated in blue and yellow, respectively. The number of cloned PCR amplicons that were sequenced is shown in brackets, and identical frame shift mutations were found in each line. No other mutations or WT alleles were found, indicating larger deletion of the second allele in all cases. **(C)** WB validation of APC protein expression using whole-cell lysates from all three organoid lines (WT and *APC*-KO). Noncropped original gel scan is shown. Actin WB serves as a loading control, and the experiment was independently performed twice. WT and truncated APC variants are indicated by black and white arrowheads, respectively. Related to Fig. 1.

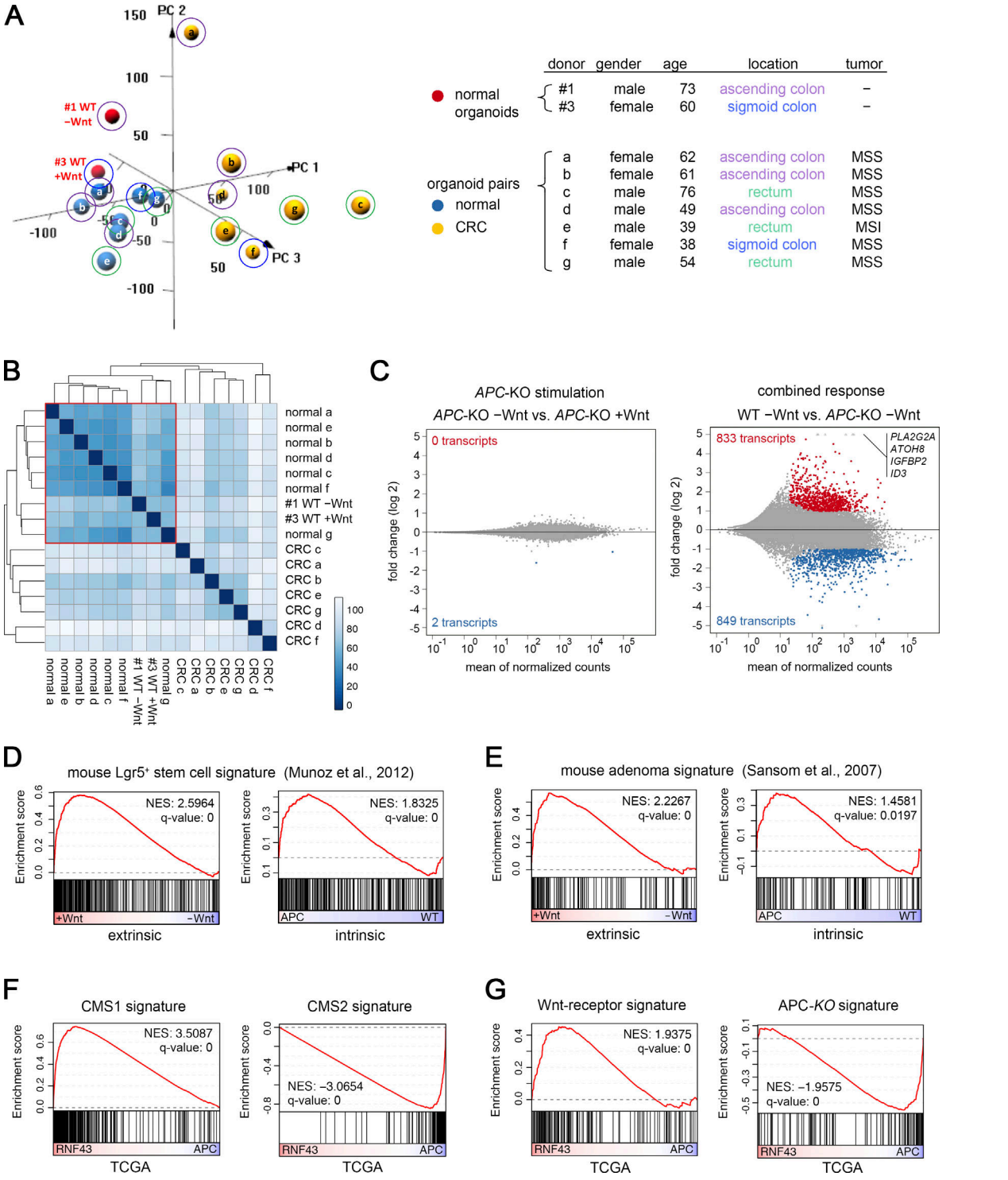

Figure S2. **Detailed characterization of transcriptomic data. (A)** PCA of organoid lines investigated in this study (red) and paired organoids lines from resected CRC tissue (yellow) or adjacent normal tissue (blue). Note that normal organoids cluster apart from CRC organoids. The 15,000 most variant genes were included for the analysis. The legend on the right displays corresponding data of the organoids. Note that the lines do not cluster according to gender, age, location (color coded; refer to circles in the PCA plot), or microsatellite stability/instability (MSS/MSI). All samples except #1 were cultured in +Wnt/R-spondin medium, and RNA sequencing was performed together for all samples to avoid batch effects. **(B)** Pairwise correlation matrix of the same data analyzed in A shows distinct clustering of all normal lines (red square). Color map shows Euclidean distance between samples. **(C)** Differential gene expression analysis. Up- and down-regulated proteins (± 1 log twofold change; P adjust < 0.05) are marked in red and blue. Note the minimal changes after *APC*-KO stimulation and the abundant changes upon combined stimulation (extrinsic and intrinsic response). **(D and E)** GSEA using previously reported mouse signatures for Lgr5⁺ stem cells (D) and mouse *APC* mutant adenoma (E). Each signature was studied in the extrinsic and intrinsic Wnt responses. **(F and G)** GSEA using TCGA expression data for colon cancer samples with somatic mutations in *RNF43* (n = 29) or *APC* mutations (n = 30). Expression signatures for CMS1 and CMS2 (F) and for the Wnt-receptor and *APC*-KO signatures (G) were studied. Related to Figs. 2 and 3.

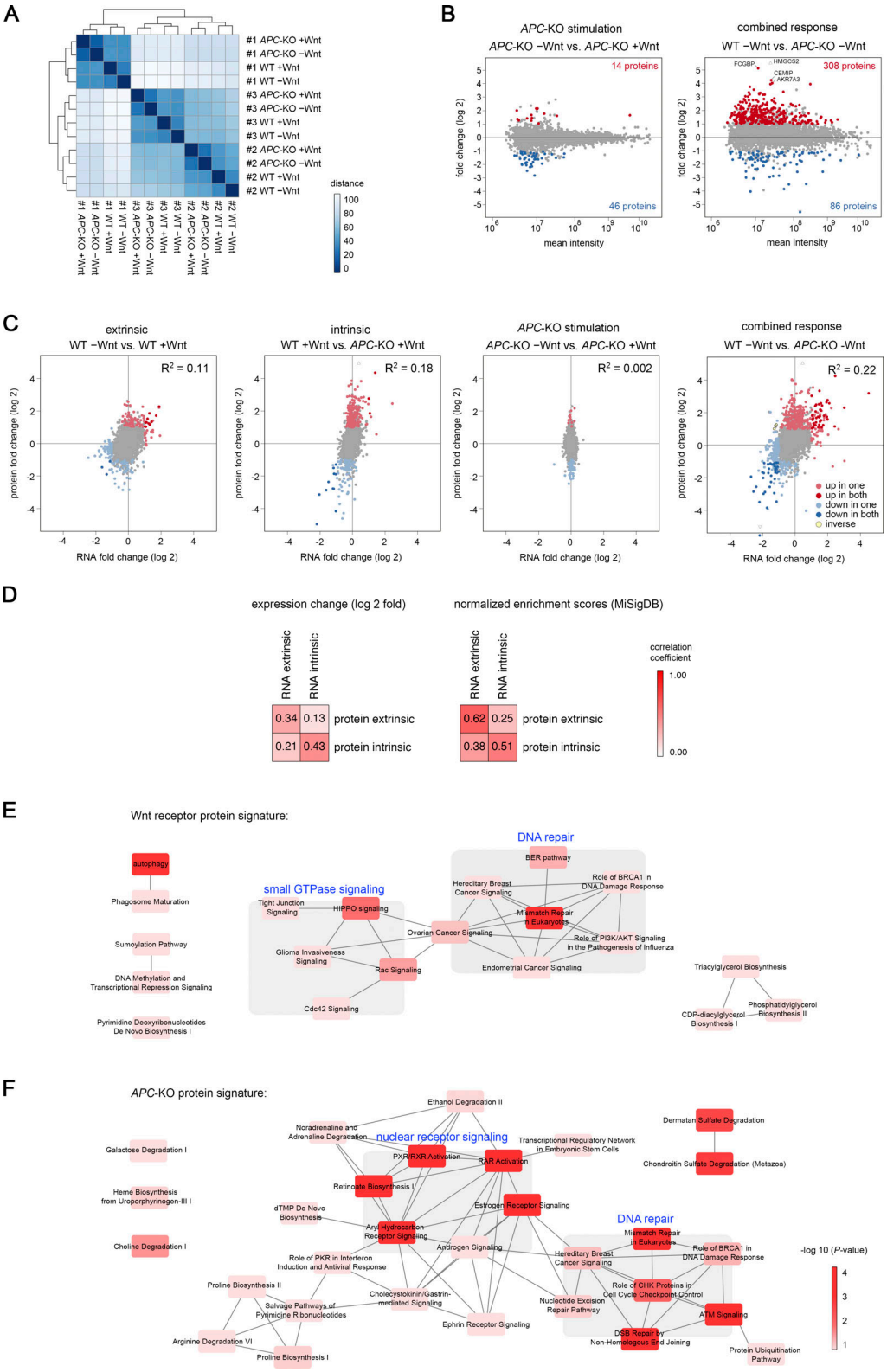

Figure S3. **Detailed characterization of proteomic data. (A)** Pairwise correlation matrix of all protein samples shows donor-specific clustering. Color map marks Euclidean distance between samples. **(B)** Differential protein expression analysis (shown as in Fig. 5 A). Note moderate changes in after *APC*-KO stimulation and abundant changes in the combined response (extrinsic plus intrinsic stimulation). **(C)** Limited global correlation of RNA and protein changes. Correlation coefficients (R^2) are shown. **(D)** Pearson correlation of RNA–protein expression changes (left) and of NESs (GSEA, right). For GSEA, KEGG and REACTOME gene sets from the Molecular Signatures database (MSigDB v6.1, curated C2) were used. Color map shows correlation coefficients (R). **(E and F)** Ingenuity pathway analysis of identified protein signatures. Network representation of significantly enriched gene ontology terms of the Wnt-receptor signature (E) and the *APC*-KO protein signature (F). Color map shows P values. Related to Figs. 5 and 6.

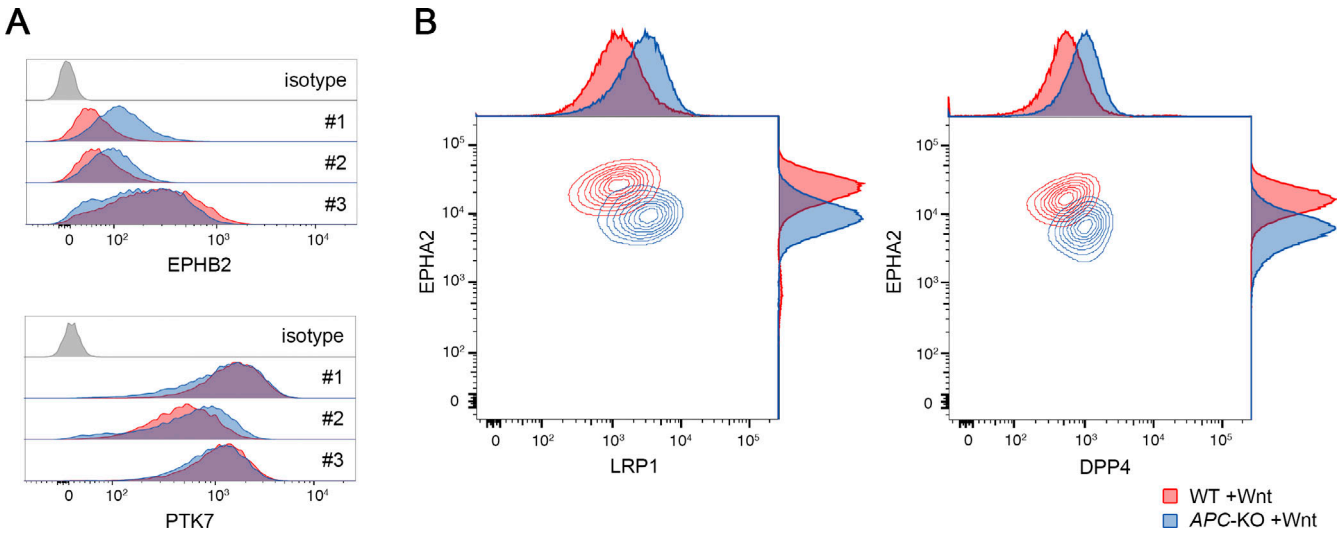

Figure S4. **Surface marker analysis in normal and *APC* mutant organoids. (A)** FACS analysis of the known stem cell surface markers EPHB2 and PTK7 that display similar expression levels on WT and *APC*-KO cells. Experiments were performed as in Fig. 7 D. **(B)** Combinatorial staining of LRP1/EPHA2 and DPP4/EPHA2 allows further separation between WT to *APC*-KO cells. All stainings (in A and B) were independently reproduced. Related to Fig. 7.

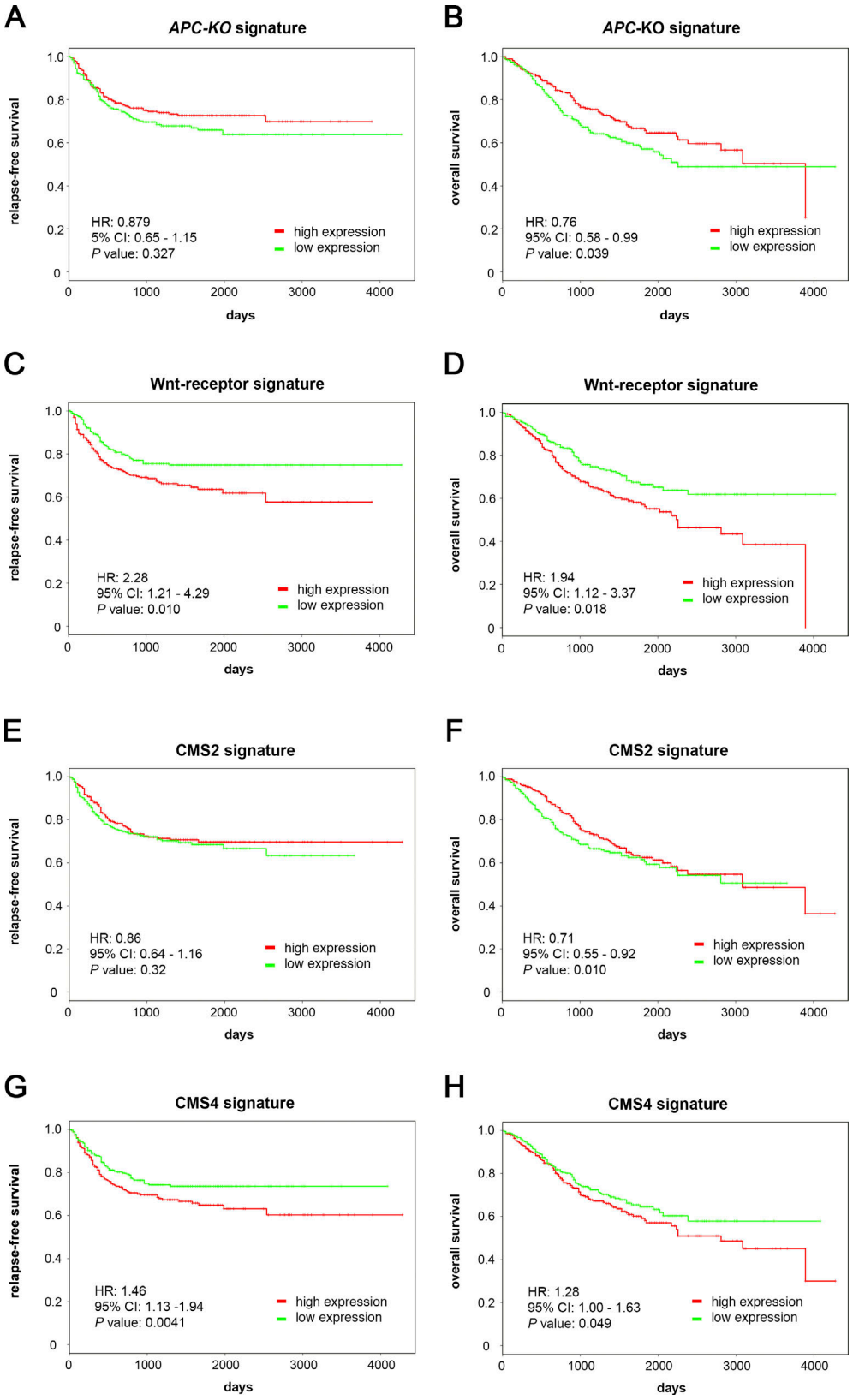

Figure S5. **Prognostic value of *APC*-KO and Wnt-receptor signatures in CRC. (A–H)** Relapse-free survival (A, C, E, and G) and overall survival (B, D, F, and H) was determined in the expression cohort GSE39582 (265 CRC cases; adjusted for stage, chemotherapy, and P53/KRAS/BRAF mutation). For each signature, the cohort was divided into high (red) and low (green) expression using the PROGgeneV2 program. Kaplan–Meier plots show hazard ratios (HR), 95% confidence intervals (CI), and P values (log-rank test, multivariate analyses). Note that *APC*-KO/CMS2 and Wnt-receptor/CMS4 signatures are linked to similar outcome. HR, hazard ratio; CI, confidence interval. Related to Fig. 8.

Table S4. **Additional information of the validated proteins in this study**

Protein abbreviation and name	Observed expression	Reported expression and molecular function in colon/tumors	Available pharmacologic inhibitors
AMACR, Alpha-methylacyl-CoA racemase	Adenoma and stem cells (validated by IHC)	Mitochondrial/peroxisomal metabolism: Catalyzes the chiral inversion of methyl groups in several lipids and drugs and regulates their metabolism. Established biomarker in prostate cancer and increased levels of AMACR have been reported in solid cancers (Lloyd et al., 2008). In CRC, increased expression in adenomas and low-grade carcinomas has been described (Shukla et al., 2017).	Several AMACR inhibitors have been described that inhibit growth of prostate cancer cell lines (Wilson et al., 2011).
CEMIP, Cell migration-inducing and hyaluronan-binding protein	Adenoma (validated by WB and IHC)	Cell signaling: Secreted enzyme that binds and hydrolyzes hyaluronic acid. Involved in motility of cancer cells. Frequently overexpressed in CRC, and knockdown in cell lines attenuated the Wnt pathway (Birkenkamp-Demtroder et al., 2011).	No inhibitor described
CHDH, Choline dehydrogenase	Adenoma (validated by WB)	Mitochondrial metabolism: Catalyzes betaine biosynthesis from choline. No reported function in cancer.	No inhibitor described
DPP4, Dipeptidyl peptidase 4	Adenoma and differentiated normal cells (validated by FACS)	Cell signaling: Cell surface glycoprotein protein (CD26) with exopeptidase activity. Previously described as marker for tumor cells (Havre et al., 2008).	Several DPP4 inhibitors are in clinical use in diabetes type 2.
HMGCS2, 3-hydroxy-3-methylglutaryl-CoA synthase 2	Adenoma (validated by WB and IHC)	Fatty acid metabolism: Mitochondrial isoform that regulates fatty acid β-oxidation and ketone-body production. Described as repression target of MYC and expressed in differentiated normal cells in human colon and downregulated in undifferentiated CRC (Camarero et al., 2006). Other report shows increased expression in progressed CRC and positive role in tumor invasiveness (Chen et al., 2017).	Two structurally unrelated inhibitors of HMGCS have been described (Nagashima et al., 1993; Pojer et al., 2006).
LRP1, Low-density lipoprotein receptor-related protein 1	Adenoma (validated by FACS)	Fatty acid metabolism: Role in cholesterol import, intracellular signaling, and endocytosis. Reduced expression of LRP-1 has been described in CRC, and low expression is correlated with poor clinical outcome (Boulagnon-Rombi et al., 2018).	No inhibitor described
PPIP5K2, Inositol hexa-kisphosphate and diphospho-inositol-penta-kisphosphate kinase 2	Adenoma and stem cells (validated by WB and IHC)	Cell signaling and metabolism: PPIP5Ks catalyze the final step in 1,5-$InsP_8$ synthesis, an inositol pyrophosphate that is involved in signaling and energy metabolism. Loss of PPIP5K1 and 2 induces a hypermetabolic, growth-inhibited phenotype in the HCT116 colon cancer cell line (Gu et al., 2017), suggesting that pharmacological targeting offers a potential approach for tumor therapy.	No inhibitor described
SCD, Acyl-CoA desaturase	Adenoma (validated by WB)	Fatty acid metabolism: enzymatic conversion of saturated fatty acids into monounsaturated fatty acids. High expression in CRC cell lines induces invasiveness and associates with poor prognosis in CRC patients (Sánchez-Martínez et al., 2015). Blockage of SCD1 suppresses proliferation and induces apoptosis in CRC cell lines (Chen et al., 2016).	Two structurally unrelated SCD inhibitors have been described (Liu et al., 2007; Roongta et al., 2011).
SMARCA5, SWI/SNF-related matrix-associated actin-dependent regulator of chromatin subfamily A5	Adenoma (validated by WB)	Chromatin remodeling: Catalytic subunit of several nucleosome-remodeling complexes that regulate transcription and replication. Contains ATP-dependent helicase activity.	No specific inhibitor described

Table S4. **Additional information of the validated proteins in this study (*Continued*)**

Protein abbreviation and name	Observed expression	Reported expression and molecular function in colon/tumors	Available pharmacologic inhibitors
SRC, Src protein tyrosine kinase	Adenoma (validated by WB)	Cell signaling: Involved in cell growth and (oncogenic) signaling. In CRC, SRC is frequently overexpressed, and high activity is correlated with dismal prognosis (Gargalionis et al., 2014). *APC* loss has been reported to upregulate SRC expression and activity in colon organoids (Taniguchi et al., 2017).	Several inhibitors for SRC family kinases with anti-tumor activity are in clinical use.

Summary of the observed expression using orthologous methods and data from previous literature on expression, function and availability of pharmacological inhibitors for each protein. IHC, immunohistochemistry.

Tables S1, S2, S3, and S5 are included online as separate Excel files. Table S1 lists identified Wnt-receptor and *APC*-KO signatures. Table S2 contains list of gRNAs, qPCR primers, and antibodies used. Table S3 describes the characterization of tissue expression using the Human Protein Atlas. Table S5 contains CMS classification and subtype-specific RNA signatures.

References

Birkenkamp-Demtroder, K., A. Maghnouj, F. Mansilla, K. Thorsen, C.L. Andersen, B. Øster, S. Hahn, and T.F. Ørntoft. 2011. Repression of KIAA1199 attenuates Wnt-signalling and decreases the proliferation of colon cancer cells. *Br. J. Cancer.* 105:552–561. https://doi.org/10.1038/bjc.2011.268

Boulagnon-Rombi, C., C. Schneider, C. Leandri, A. Jeanne, V. Grybek, A.M. Bressenot, C. Barbe, B. Marquet, S. Nasri, C. Coquelet, et al. 2018. LRP1 expression in colon cancer predicts clinical outcome. *Oncotarget.* 9:8849–8869. https://doi.org/10.18632/oncotarget.24225

Camarero, N., C. Mascaró, C. Mayordomo, F. Vilardell, D. Haro, and P.F. Marrero. 2006. Ketogenic HMGCS2 Is a c-Myc target gene expressed in differentiated cells of human colonic epithelium and down-regulated in colon cancer. *Mol. Cancer Res.* 4:645–653. https://doi.org/10.1158/1541-7786.MCR-05-0267

Chen, L., J. Ren, L. Yang, Y. Li, J. Fu, Y. Li, Y. Tian, F. Qiu, Z. Liu, and Y. Qiu. 2016. Stearoyl-CoA desaturase-1 mediated cell apoptosis in colorectal cancer by promoting ceramide synthesis. *Sci. Rep.* 6:19665. https://doi.org/10.1038/srep19665

Chen, S.-W., C.-T. Chou, C.-C. Chang, Y.-J. Li, S.-T. Chen, I.-C. Lin, S.-H. Kok, S.-J. Cheng, J.-J. Lee, T.-S. Wu, et al. 2017. HMGCS2 enhances invasion and metastasis via direct interaction with PPARα to activate Src signaling in colorectal cancer and oral cancer. *Oncotarget.* 8:22460–22476.

Gargalionis, A.N., M.V. Karamouzis, and A.G. Papavassiliou. 2014. The molecular rationale of Src inhibition in colorectal carcinomas. *Int. J. Cancer.* 134:2019–2029. https://doi.org/10.1002/ijc.28299

Gu, C., H.N. Nguyen, D. Ganini, Z. Chen, H.J. Jessen, Z. Gu, H. Wang, and S.B. Shears. 2017. KO of 5-InsP$_7$ kinase activity transforms the HCT116 colon cancer cell line into a hypermetabolic, growth-inhibited phenotype. *Proc. Natl. Acad. Sci. USA.* 114:11968–11973. https://doi.org/10.1073/pnas.1702370114

Havre, P.A., M. Abe, Y. Urasaki, K. Ohnuma, C. Morimoto, and N.H. Dang. 2008. The role of CD26/dipeptidyl peptidase IV in cancer. *Front. Biosci.* 13:1634–1645. https://doi.org/10.2741/2787

Liu, G., J.K. Lynch, J. Freeman, B. Liu, Z. Xin, H. Zhao, M.D. Serby, P.R. Kym, T.S. Suhar, H.T. Smith, et al. 2007. Discovery of potent, selective, orally bioavailable stearoyl-CoA desaturase 1 inhibitors. *J. Med. Chem.* 50:3086–3100. https://doi.org/10.1021/jm070219p

Lloyd, M.D., D.J. Darley, A.S. Wierzbicki, and M.D. Threadgill. 2008. Alpha-methylacyl-CoA racemase--an 'obscure' metabolic enzyme takes centre stage. *FEBS J.* 275:1089–1102. https://doi.org/10.1111/j.1742-4658.2008.06290.x

Nagashima, H., H. Kumagai, H. Tomoda, and S. Omura. 1993. Inhibition of hepatic cholesterol biosynthesis by a 3-hydroxy-3-methylglutaryl coenzyme A synthase inhibitor, 1233A, in mice. *Life Sci.* 52:1595–1600. https://doi.org/10.1016/0024-3205(93)90060-G

Pojer, F., J.-L. Ferrer, S.B. Richard, D.A. Nagegowda, M.-L. Chye, T.J. Bach, and J.P. Noel. 2006. Structural basis for the design of potent and species-specific inhibitors of 3-hydroxy-3-methylglutaryl CoA synthases. *Proc. Natl. Acad. Sci. USA.* 103:11491–11496. https://doi.org/10.1073/pnas.0604935103

Roongta, U.V., J.G. Pabalan, X. Wang, R.-P. Ryseck, J. Fargnoli, B.J. Henley, W.-P. Yang, J. Zhu, M.T. Madireddi, R.M. Lawrence, et al. 2011. Cancer cell dependence on unsaturated fatty acids implicates stearoyl-CoA desaturase as a target for cancer therapy. *Mol. Cancer Res.* 9:1551–1561. https://doi.org/10.1158/1541-7786.MCR-11-0126

Sánchez-Martínez, R., S. Cruz-Gil, M. Gómez de Cedrón, M. Álvarez-Fernández, T. Vargas, S. Molina, B. García, J. Herranz, J. Moreno-Rubio, G. Reglero, et al. 2015. A link between lipid metabolism and epithelial-mesenchymal transition provides a target for colon cancer therapy. *Oncotarget.* 6:38719–38736. https://doi.org/10.18632/oncotarget.5340

Shukla, N., A.K. Adhya, and J. Rath. 2017. Expression of Alpha - Methylacyl - Coenzyme A Racemase (AMACR) in Colorectal Neoplasia. *J. Clin. Diagn. Res.* 11:EC35–EC38. https://doi.org/10.7860/JCDR/2017/25303.9727

Taniguchi, K., T. Moroishi, P.R. de Jong, M. Krawczyk, B.M. Grebbin, H. Luo, R.-H. Xu, N. Golob-Schwarzl, C. Schweiger, K. Wang, et al. 2017. YAP-IL-6ST autoregulatory loop activated on APC loss controls colonic tumorigenesis. *Proc. Natl. Acad. Sci. USA.* 114:1643–1648. https://doi.org/10.1073/pnas.1620290114

Uhlén, M., L. Fagerberg, B.M. Hallström, C. Lindskog, P. Oksvold, A. Mardinoglu, Å. Sivertsson, C. Kampf, E. Sjöstedt, A. Asplund, et al. 2015. Proteomics. Tissue-based map of the human proteome. *Science.* 347:1260419. https://doi.org/10.1126/science.1260419

Wilson, B.A.P., H. Wang, B.A. Nacev, R.C. Mease, J.O. Liu, M.G. Pomper, and W.B. Isaacs. 2011. High-throughput screen identifies novel inhibitors of cancer biomarker α-methylacyl coenzyme A racemase (AMACR/P504S). *Mol. Cancer Ther.* 10:825–838. https://doi.org/10.1158/1535-7163.MCT-10-0902